AL-MUKHTAR JOURNAL OF ENGINEERING RESEARCH ISSN online: 2519-6839 // ISSN Print 2519-6820
Vol. 6, No. (1):38-49 Available at mjer.omu.edu.ly
Received June 13, 2022, Accepted October 11, 2022, Published December, 2022 DOI: https://doi.org/10.54172/jjbdb418

NUMERICAL AND EXPERIMENTAL INVESTIGATION OF THE TRANSIENT MOTION OF A SETTLING SPHERE

Jabir Alsakit, Husam Elghannay, Hamza Failoug, Mousa Hashash, and Othman Espag

Department of Mechanical Engineering, University of Benghazi, Benghazi, Libya.

Abstract

This work aims to experimentally and numerically study the transient motion of a sphere falling in liquids. The different force models that represent different contributions to the total force are described. These "point mass" force models are introduced into the equations of motion of a moving sphere/spherical particle which can be solved numerically. A MATLAB® code is developed for this purpose and is validated with published experimental data and showed a very good agreement at a wide range of Reynolds' numbers and density rations. The experimental part is intended to be performed using available technologies that we use in our daily lives. Digital videos are recorded at a known framerate and are analyzed using an open-source video analysis software "Tracker". The experiments were performed at two different outer cylinder diameters to examine the effect of the confinement on the steady-state condition (namely the terminal velocity). Different spheres with different properties were tested along with two different fluids (oil and water). Results from the current experiment are validated with the developed code results and reasonably good agreement was obtained. Different wall correction formulas were testes and the formula of Landenburg was found to give better agreement with most of the current results. The effect of the experimental uncertainty on both the transient and steady-state results were examined and found to be insignificant for the steady-state condition and insignificant for the transient behavior.

الملخص العربي

يهدف هذا العمل لدراسة الحركة الانتقالية لكرة ساقطة في سائل ساكن معملياً وعددياً. عند الحل العددي فإن القوة الكلية يتم تجزئتها لمجموعة من النماذج المنفصلة التي تصف اسهامات مختلفة لمكونات القوة الكلية. تم توصيف النماذج ذات العلاقة و ادراجها في معادلة الحركة للكرة – او الجسيمات الكروية– التي يُراد حلها عددياً. تم التحقق من الحل العددي بمقارنته بالعديد من النتائج المعملية المنشورة و تحصلنا على مقارنة جيدة جداً على مدى واسع من رقم رينولدز ونسب كثافات الكرة للسائل. يهدف الجزء المعملي للحصول على قراءات معملية باستخدام التقنية المتاحة في حياتنا الاعتيادية حيث تم تسجيل مقاطع سقوط الكرات باستخدام كاميرا الهاتف المحمول و تحليلها باستخدام برنامج تحليل بيانات متاح مجاناً (Tracker). لغرض اختبار ظروف مختلفة تم تجربة عدد من الكرات في سائلين مختلفين (ماء وزيت) واسقاطها في اسطوانتيه بقطرين مختلفين. قورنت النتائج المعملية المتحصل عليها بتنبؤات الحل العددي وكانت نتائج المقارنة جيدة. أختبرت بعض صيغ معاملات تصحيح معامل الجرف ووجد بأن معامل لاندنبيرغ هو الأنسب لتصحيح معظم التجارب الحالية. تحاليل عدم وثوقية القياسات المعملية اثبتت ان وجود تفاوت محدود في القياسات لا يؤثر على النتائج عند الوصول لحالة الاستقرار وهو غير مؤثر بشدة في السلوك الانتقالي.

Key words: Free fall of spheres; particle equation of motion; point mass force models; experimental validation; wall correction factors.

1. Introduction

The unsteady motion of spherical particles is a classic problem with a variety of applications involving particulate flows either in natural or industrial systems. In a wide range of multiphase flow systems, particles or bubbles can fairly be approximated as spheres with subtle modifications hence the importance of studying the unsteady motion of spherical particles. Hydrodynamic or aerodynamic forces during the settlement of a sphere can be observed in a wide range of other phenomena in nature from multiphase flow to spray combustion, pollution control, boiling and bubble dynamics, sedimentation, and erosion of turbine blades. All these problems are concerned with the interaction of particles with fluids, which requires accurate knowledge of all hydrodynamic forces acting on a particle.

One of the earliest systematic investigations of the different parameters which affect the transient portion of a sphere sedimenting from rest at moderately low Reynolds numbers (Re_p < 2000) is made by Moorman [1]. The spheres were released using a magnetic release mechanism and thus nylon and aluminum spheres used in the experiment employed magnetic inserts. Different mixtures of glycerin and water are used to obtain a transparent fluid at different viscosities. The used camera has a frame rate ranging between 10-100 fps. To prevent overlaps of images at low Reynolds numbers a rotation mechanism was used to rotate the camera at about 2 rpm.

Mordant and Pinton [2] experimentally studied the unsteady motion of spherical beads (diameters ranging from 0.5 mm to 6 mm) of different materials released from rest. The beads settled in a wide bath of water having terminal Reynold's number ranging from about 40 to 8000. The bead velocity was measured using the acoustic technique and the ultrasound signal from the transducer is processed and filtered to obtain the velocity measurement.

Ten Cate et al. [3] experimentally and computationally studied the fall of a sphere at particle's Reynolds numbers ranging from ~1.5 -32. They used a 15 mm nylon ball falling in a confined container that has a width of about nine times the ball diameter to allow comparison with the computational simulations. The spheres were held in place using a vacuum in a pipette. Different types of silicone oils were used as the working fluid. The images of the falling sphere, recorded at frame rates ranging from 60 to 250, were used to determine the position of the sphere at pixel accuracy and sub-pixel displacements were estimated using fitting techniques.

Rostami et al. [4] captured the motion of falling and rebounding spheres in water using a high-speed camera (frame rate of 500 and 1000 fps). The motion of the spheres was analyzed using the software of the used high-speed camera.

More recently, Nasab [5], studied the sedimentation of 5 mm spheres with different materials falling in water in a transparent cylinder of 20 cm inner diameter. The trajectories of the falling spheres were recorded using a high-speed camera at 750 fps and the recorded sequence was analyzed using the MATLAB image processing tool.

Akhlis et al. [6] used an open-source video analysis software (Tracker) to estimate the viscosity of a fluid. The method depends on the estimation of the terminal velocity of spheres falling in a transparent cylinder. The experiment is repeated to reduce the experimental uncertainties. Good agreement was achieved when the approach was tested on Glycerin with an about 8% difference. Besides the discussed reasons to justify the difference between the reference and obtained values, the inner diameter of the cylinder is seemingly not much larger than the used spheres which may have caused some of the discrepancies.

The objective of this work is to show that using currently available technologies with not many sophisticated techniques it is possible to obtain reasonably accurate predictions of the unsteady part of a settling sphere in liquids. No sophisticated techniques will be used in this work but simply recording the motion using a digital camera of a cell phone and analyzing the motion using the open-source video analysis software. An investigation of the effect of container size will also be provided in this work.

2. Mathematical Formulation

In dynamics, Newton's second law is used to describe the motion of a rigid body. One way of simulating a moving object in a continuum fluid is by integrating the forces around its surface and using the integrated force to update the velocity and position of the object. Such resolved flow simulation requires a computational grid that is smaller than the length scale of the object (diameter in the case of spheres). Such a technique limits the applicability of this approach to a relatively small number of particles or relatively short run times. Alternatively, point mass force models can be used to represent different contributions of the fluid on the particles. In this technique, the total force is assumed to be a linear combination of different contributions. Newton's law of motion, when applied to a moving object (sphere in this case) in a stagnant fluid, has the form [7]:

$$\frac{d\vec{v}}{dt} = (1-\frac{\rho_f}{\rho_p})\vec{g} + \frac{3C_D\rho_f}{4d\rho_p}\vec{v}^2 + C_\forall\frac{\rho_f}{\rho_p}\left(\frac{d\vec{v}}{dt}\right) - \frac{18\pi\nu_f\rho_f}{d^2\rho_p}\int_0^t K(t-\tau)\frac{d\vec{v}(\tau)}{d\tau}d\tau \quad (1)$$

where the forces are per unit mass of the particle. The terms on the right-hand side are due to the net weight of the particle (gravity-bouncy), drag, added mass, and history force, respectively.

The drag force accounts for the quasi-steady viscous dissipation due to skin friction and form drag. The added mass effect accounts for the force required to accelerate/decelerate the fluid surrounding the particle, whereas the history force model accounts for the temporal

evolution of the viscous region near the particle (boundary layer) when the particle undergoes unsteady motion.

In Eq. (1) v is the fluid velocity, g is the gravitational acceleration, $\rho_f, \rho_p, \nu_f, C_d, g$ and d are the fluid density, particle density, the fluid kinematic viscosity, the drag coefficient, the gravitational acceleration, and the particle diameter. C_v is the added mass coefficient which is equal to 0.5 for a spherical particle.

A common and reasonably accurate approximation for the drag of particles with laminar and transitional wakes is given by the Schiller-Naumann drag formula [8] whose Stokes correction is given by;

$$C_D = \begin{cases} \dfrac{24\left(1 + 0.15Re_p^{0.687}\right)}{Re_p}, & Re_p < 1000 \\ 0.44, & Re_p \geq 1000 \end{cases} \quad (2)$$

in which the particle Reynolds number Re_p is calculated as;

$$Re_p = \frac{d|\vec{v}|}{\nu_f} \quad (3)$$

The integration kernel in the history force model, K, can be expressed as [7]:

$$K_M(t-\tau) = \left\{ \left(4\pi \frac{(t-\tau)}{\tau_d}\right)^{\frac{1}{2c_1}} + \left(\pi \frac{(t-\tau)^2}{\tau_d^2}\left(\frac{Re_p(\tau)}{0.75 + c_2 Re_p(\tau)}\right)^3\right)^{\frac{1}{c_1}} \right\}^{-c_1} \quad (4)$$

For finite Reynold's numbers, Mei and Adrian [9] proposed constants c_1 = 2 and c_2 = 0.105 based on their resolved simulations of oscillating flow. Other researchers suggested slightly different values for c_1 and c_2. τ_d is the diffusive time scale of the particle defined as [7];

$$\tau_d = \frac{d^2}{\nu_f} \quad (5)$$

Among all force models in Eq. (1) the history force is the most computationally demanding contribution since it requires storing and using all past information of particle velocity from the start of the particle motion to the current instant. It should be noted that other forces such as lift, Saffman's, Brownian, and thermo-pheretic are not discussed in this work since they are not relevant and the reader is referred to some multiphase flow textbook [10] for further reading. If the fluid is not stagnant then the relative velocity should be used instead of the particle velocity in all the above formulations.

3. Computer Program Validation

A MATLAB® program is developed to numerically solve Eq. (1). Validation of the computer code with published is provided to gain trust of the code result before using it to validate the experiments conducted in the current work. The code is validated with measurements of the motion of a settling particle released from rest. The spheres are released from rest and will start gaining some velocity as time advances. Due to the (now considerable) drag force and presumably long time, there will be a situation in which an equilibrium is achieved between the drag force and the net weight of the sphere. At this condition, the sphere will be moving at constant velocity which is called "terminal velocity". The terminal velocity can be used to validate the results besides the validation of the transient part of the velocity from rest to terminal velocity.

The selected experiments in this section are from the work of [1-3]. The velocity variation in the figures is normalized by the terminal velocity, and time is normalized by the diffusion time (as per Eq. (5)) as given in Table 1. The results cover a range of terminal Reynolds numbers ranging from nearly 1 to about 280 with density ratios ranging from about 1.16 -9.2. The Simulation results are presented in such cases where only drag and gravity forces are active, drag, gravity, and added mass forces are active, and when all forces are active.

Table 1: Sphere and fluid properties for the selected experiments [1-3]

Run#	$Re_{p.term}$	d (mm)	ρ_p (kg/m^3)	ρ_f (kg/m^3)	ν_f (m^2/s)
10	31.5	11.1	7782.2	850.4	2.7×10^{-4}
19	181	15.88	3076.8	834.9	7.2×10^{-5}
21	67	9.51	3076.8	834.9	7.2×10^{-5}
22	28	6.37	3076.8	843.9	7.2×10^{-5}
27	29	12.71	3076.8	1247.2	1.49×10^{-4}
29	6	6.37	3076.8	1247.2	1.49×10^{-4}
30	4.2	6.37	3076.8	1252.4	1.88×10^{-4}
31	0.9	6.37	3076.8	1257.5	4.49×10^{-4}
E1	1.5	15	1120	970	3.85×10^{-4}
E2	4.1	15	1120	965	2.2×10^{-4}
M4	260	0.8	7710	1000	1×10^{-6}

The experiment should be compared to the case where all forces are activated. The sphere eventually reaches the steady state with a velocity equal to its terminal velocity. Figures 1 shows a comparison of simulations at different density ratios ($S = \rho_f / \rho_p$) of 3.7. The abbreviation "AM" indicates that the added mass force is activated along with the net weight and drag forces whereas the abbreviation "All" means all force components in Eq. (1) are active. It can be seen that the inclusion of additional force models leads to an improvement in the prediction as compared to the experimental results.

Figure 2 presents the validation at a lower density ratio of 2.47 and a lower Reynold's number. In these cases, the effect of history force is even more pronounced. The predictions are in reasonably good agreement with the experiment under these conditions. At a rather lower density ratio (S~1.16) and yet at a low Reynolds number the good agreement is still reserved as can be seen from Figure 3.

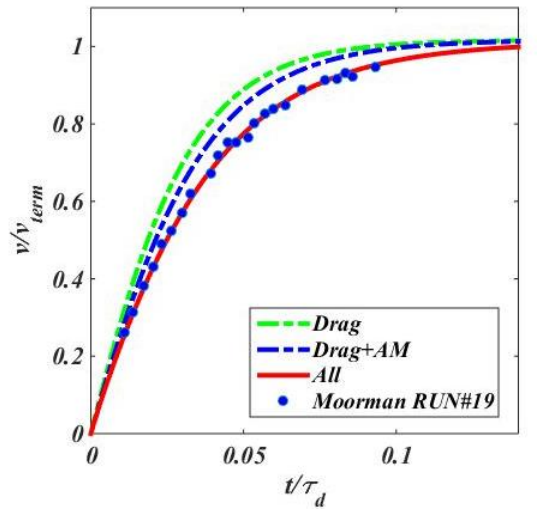

(a)

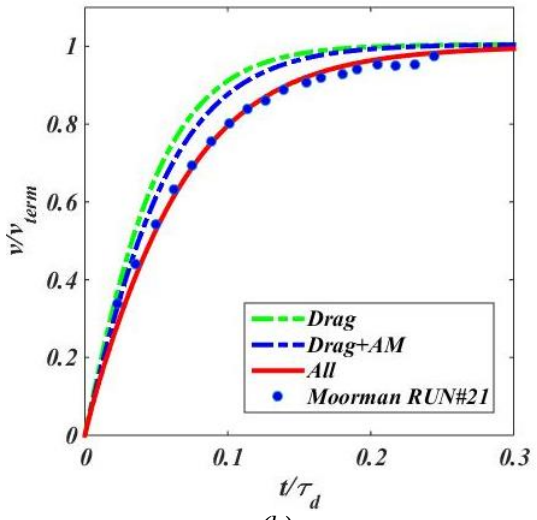

(b)

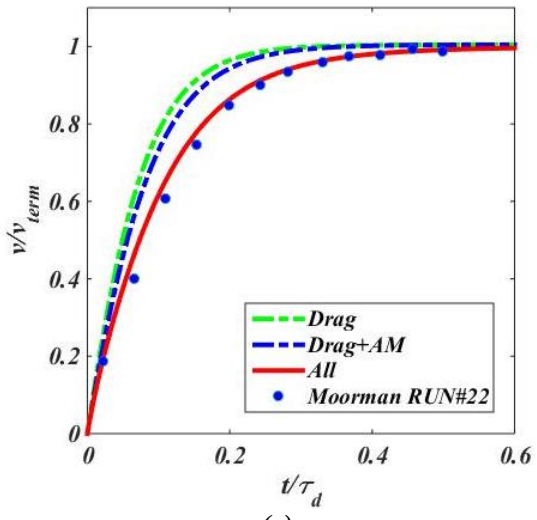

(c)

Fig. 1: Comparison of experiment with current model at constant density ratio (S~3.7) and different Reynolds numbers *a)* Re_p = 181, *b)* Re_p = 67, and *c)* Re_p = 28

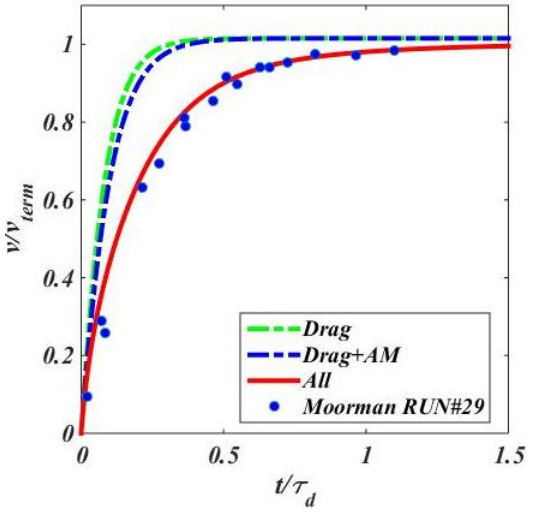

(a)

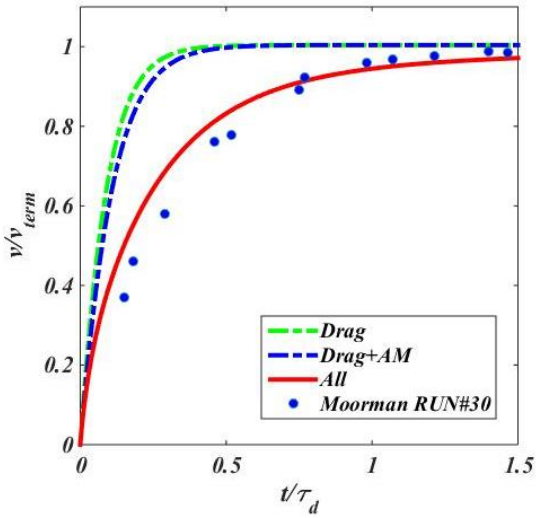

(b)

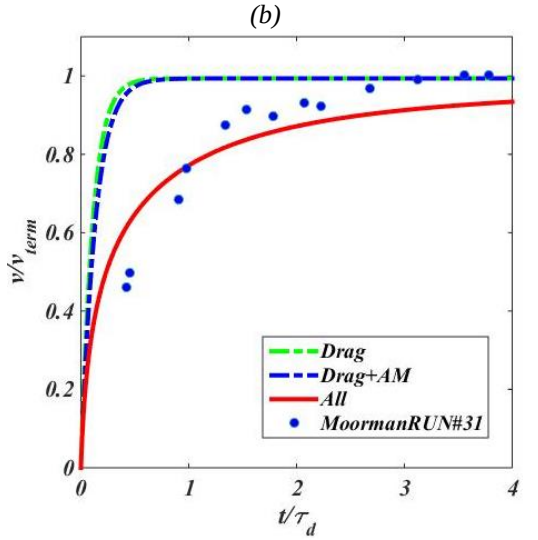

(c)

Fig. 2: Comparison of experiment with current model at constant density ratio (S~2.47) and different Reynolds numbers *a)* Re_p = 6, *b)* Re_p = 4.2, and *c)* Re_p = 0.9

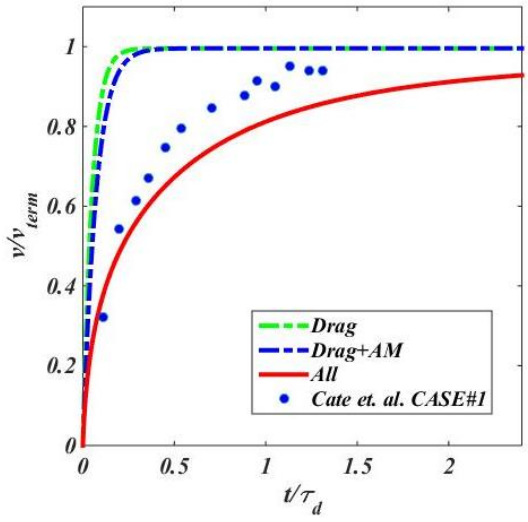

(a)

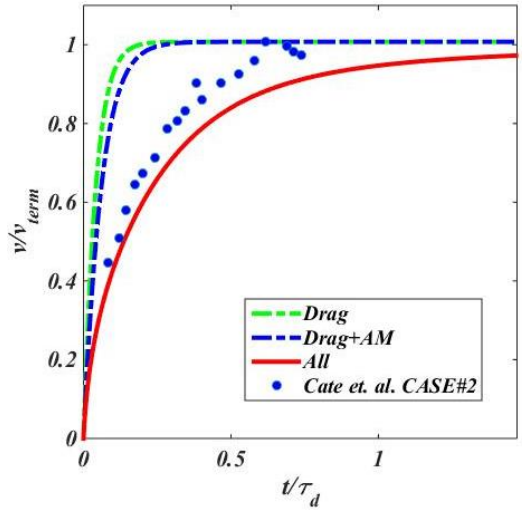

(b)

Fig. 3: Comparison of experiment with current model at constant density ratio (S~1.16) and different (low) Reynolds numbers *a)* Re_p = 1.5, and *b)* Re_p = 4.1

Figure 4 shows the results at Re_p ~29 and different density ratios (2.4-9.2). While the effect of the history force is increased with the decrease of the density ratio, the agreement between the experiment and the code predictions is preserved. Figure 5 shows a comparison of experiments at a Reynolds number of 260 where the predictions are in agreement with the experiment. As can be seen, the effect of the history force gets reduced with the increase of Reynolds number and thus no further higher Reynolds numbers have been tested. The numerical solution over-predicts the total force on the case of low Reynolds numbers and low density ratios such as the selected cases of Ten Cate et al. (Figure 3).

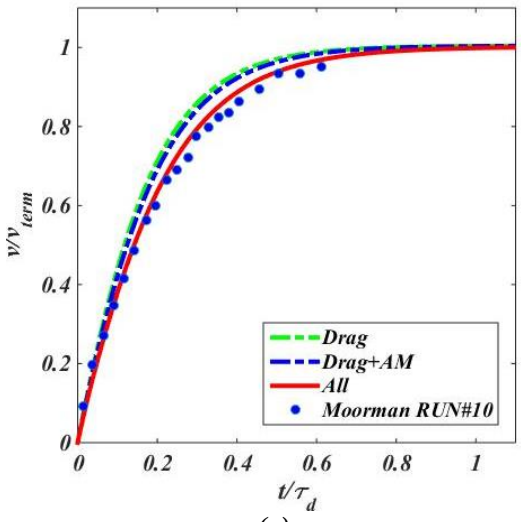

(a)

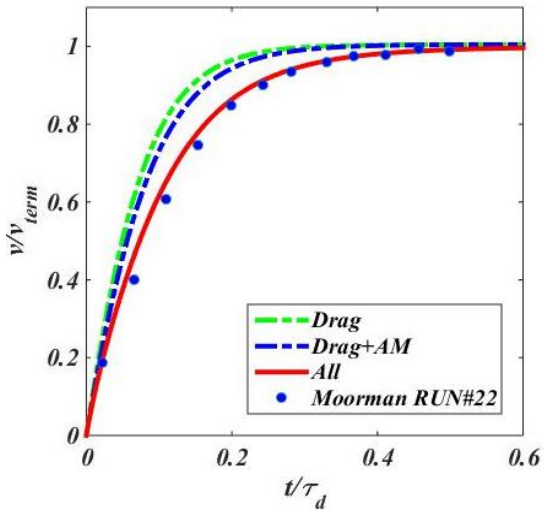

(b)

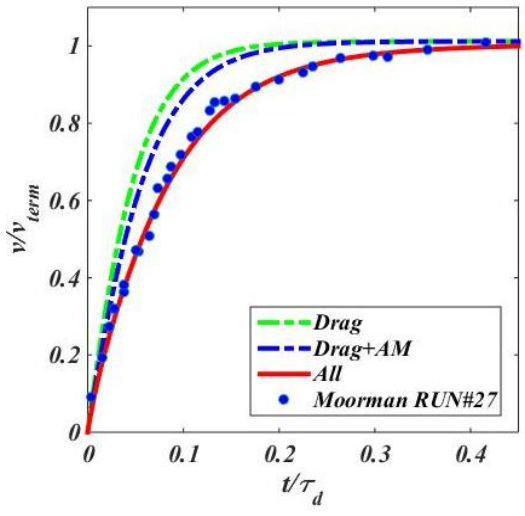

(c)

Fig. 4: Comparison of experiment with current model at Reynolds Number Re_p ~29 and different density ratios. *a)* S = 9.2, *b)* S = 3.7, and *c)* S = 2.4

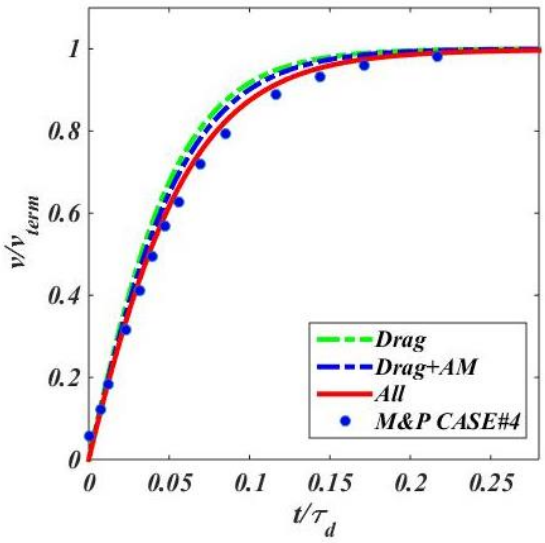

Fig. 5: Comparison of current model at Re = 260 & S= 7.71

Generally speaking, the drag force is dominant as Reynold's number is getting higher and it is expected that at some even higher Reynolds number than currently tested cases the drag force might reasonably predict the unsteady behavior. The added mass effect, however, is the same since the density ratio is kept the same. In the case of free fall both the added mass and history force resist acceleration, and, consequently, they decrease the rate of acceleration of the spheres. The experimental results are in very good agreement with the experiment where the effect of the history force is increased with the reduction of Reynolds' number.

4. Experimental Work

The purpose of this section is to capture the transient motion of spheres falling in liquids and compare it with the prediction of the developed code. The apparatus required in this part is a -glass-graduated cylinder (two different inner diameters were used), spheres with different properties, digital camera. The camera of a cell phone (Xiaomi-Poco F2 model) was used since it allowed capturing videos at a frame rate of 60-1000. Additional tools, which are handy in performing the experiment, are white background, an additional light source (directed to the whiteboard), a magnet to facilitate picking the steel spheres from the fluid (oil or water), and a release mechanism. This study made use of a falling ball viscometer to estimate the viscosity of the used oil. Although oil (SAE 20W50 with a commercial brand name LUKE-Oil) was primarily employed, the fall of spheres in water was tested in a few cases (a glass sphere in water). Difficulties in tracking high-speed spheres eliminated using steel spheres with water and difficulties in tracking the transparent glass sphere discourage performing additional tests.

4.1 Experimental results

Figure 6 shows the experimental setup of the narrow and wide cylinders. One of the tested release mechanisms can be seen in figure 6a. The sphere should be submerged totally before its release. The camera is fixed at a stationary point from the apparatus. To avoid air entertainment, the particles were initially submerged and held in a place under the oil surface and then released. Four different spheres from the falling ball viscometer kit were used. The properties of the used spheres as extracted from the manufacturer's manual are listed in Table 2.

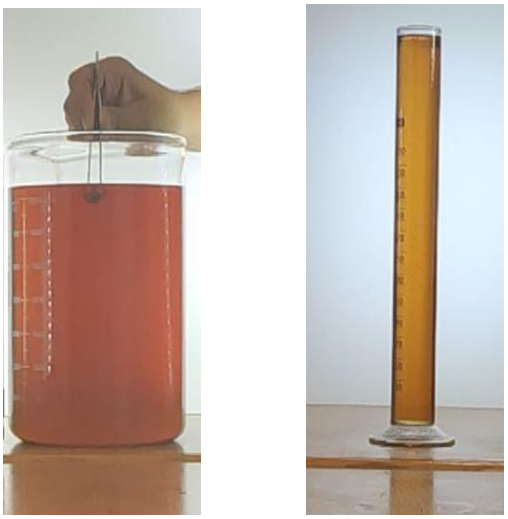

(a) *(b)*

Fig. 6: Experimental setup *(a)* wide, and *(b)* narrow graduated cylinder

Table 2: Properties of the used spheres

Ball	Diameter (mm)	Weight (g)	Density (g/cm^3)	Material
1	15.66	4.455	2.221	Glass
2	15.25	16.285	8.140	Steel
3	11.12	5.563	7.734	Steel
4	15.62	16.285	8.153	Steel

A high-speed camera was used to record the trajectory of the spheres. This camera is capable of delivering videos at different frames per second (60fps – 120fps – 240fps) and also higher frames with different resolutions. The captured video captures the moment of the release of the ball until the moment it reaches the bottom of the cylinder. The video is taken and processed using "Tracker" [11] which analyzes and extracts the required data after calibration of one initial view. The experimental data is imported to the MATLAB® for comparison purposes.

Table 3 lists fluid and sphere properties along with the predicted and measured terminal velocity of the different experiments. The experimental value was obtained by averaging the last few data points of the experiment. The parameter d/*D* stands for the ratio of the sphere diameter to the inner diameter of the graduated cylinder. The inner diameter (D) in this work was 40 mm for Runs 1-4 and 160 mm for Runs 5-9. The last column provides the difference between the measured and predicted values of the terminal velocities. All reported experiments are recorded at a frame rate of 240 fps except for run 2b which is recorded at 60 fps. It can be seen that all experiments with a narrow graduated cylinder (Runs #1-4) have a terminal velocity that is lower than predicted by the code. The listed code results don't take into account the presence of a nearby wall [12, 13]. The effect of the wall is to increase the drag coefficient and thus reduce the terminal velocity. Deviations of the values of the terminal velocity from the experiment are getting less at the wide graduated cylinder. As can be seen, experiment (Run-1) has the least deviation since it has a diameter ratio of *d/D* as the smallest diameter ball is used. As will be seen later the wall effect of the wider graduate cylinder has a less significant effect on the terminal velocity.

Table 3: Sphere and fluid properties for the selected settling sphere experiments

Run#	Ball #	ρ_f (kg/m^3)	ν_f (mm^2/s)	d/D (%)	$V_t\left(\frac{m}{s}\right)$		% |diff.|
					Exp.	Code	
1	3	840	418	27.8	0.57	0.64	12
2a	4	840	367	39.1	0.686	1.038	51
2b	4	840	367	39.1	0.715	1.038	45
4	1	840	367	39.2	0.173	0.313	81
5	3	850	500	7	0.571	0.581	1.8
6a	2	850	500	9.5	0.862	0.885	2.7
6b	2	850	500	9.5	0.864	0.885	2.4
8	1	850	500	10	0.224	0.259	16
9a	1	998	1	10	0.66	0.74	12
9b	1	998	1	10	0.6	0.74	23

Figures 7-13 show the transient variation of the velocity from the moment of its release until reaching the steady-state condition where the velocity comes to a steady value. The plots are presented in non-dimensional representation for generality. Although the predicted results may indicate that the particle almost reached its terminal velocity, some experiments may have not yet reached this condition (e.g. Run #6). The reason for that is because of the short fall distance, especially for the wide cylinder. The estimated fall distance for the narrow and wide cylinders is roughly 19 cm and 25 cm respectively.

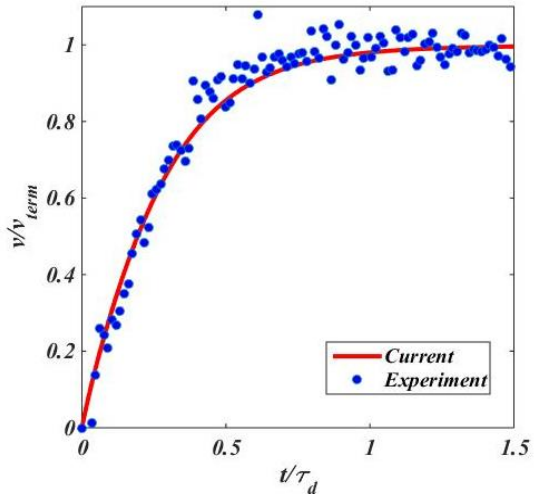

Fig. 7: Transient behavior to steady-state for Run#1 ($Re_{p,term}$ ~17, S~9.2)

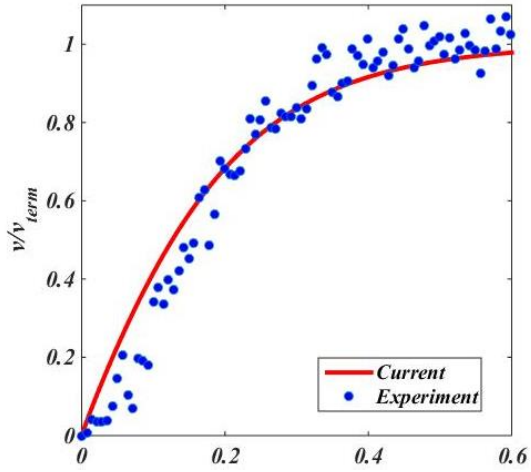

(a)

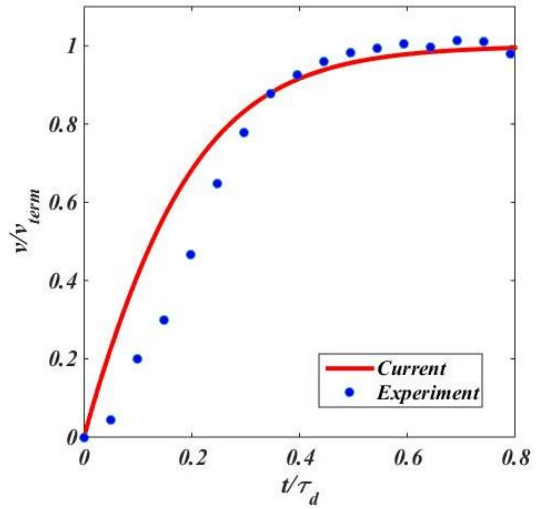

(b)

Fig. 8: Transient behavior to steady-state for the same conditions ($Re_{p,term}$ ~44, S~9.7) at different frame rates *(a)* Run#2a (240 fps), *(b)* Run#2b (60 fps)

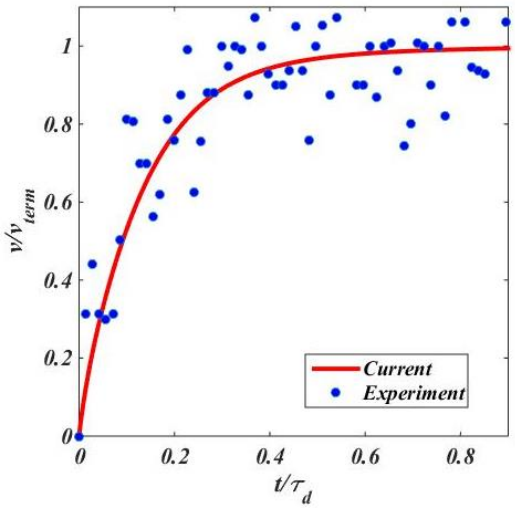

Fig. 9: Transient behavior to steady-state for Run#4 ($Re_{p,term}$ ~13, S~2.6)

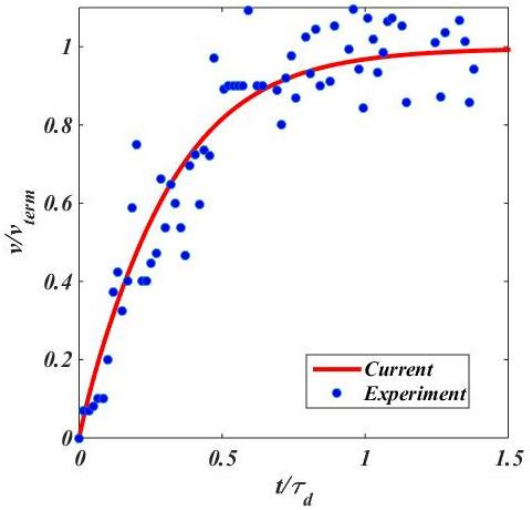

Fig. 10: Transient behavior to steady-state for Run#5 ($Re_{p,term}$ ~13, S~9.1)

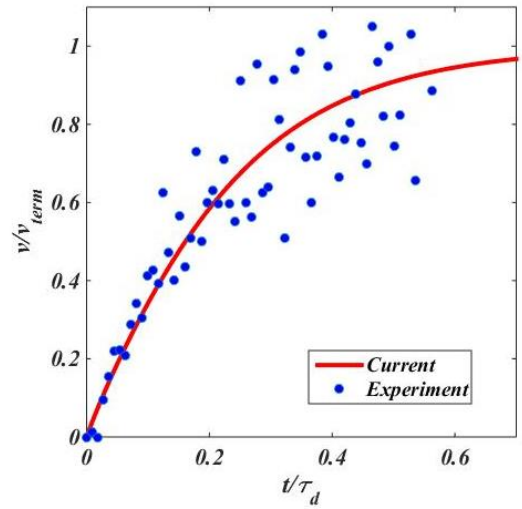

(a)

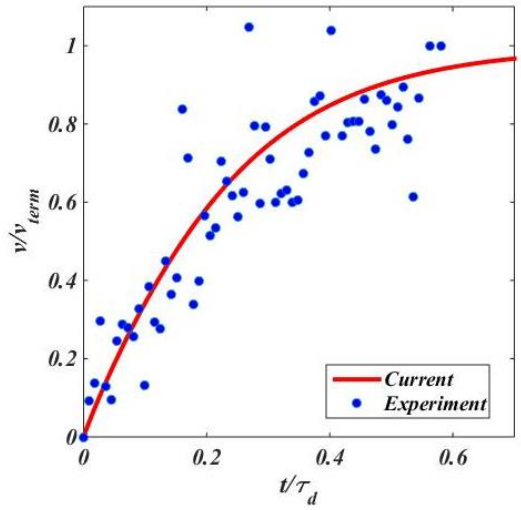

(b)

Fig. 11: Transient behavior to steady-state for the same conditions ($Re_{p,term}$ ~27, S~9.6) of Runs *(a)* 6a and *(b)* 6b

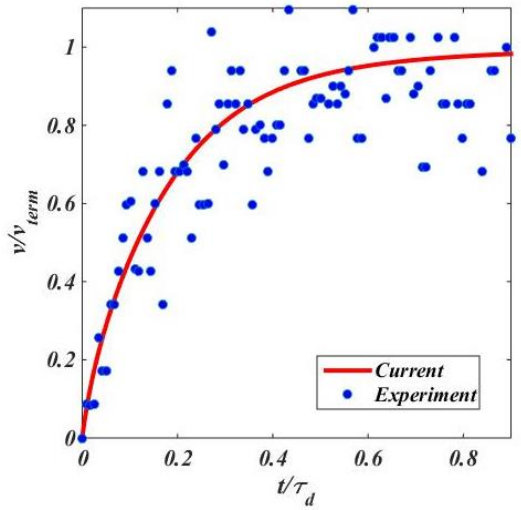

Fig. 12: Transient behavior to steady-state for Run#8 ($Re_{p,term}$ ~8, S~2.6)

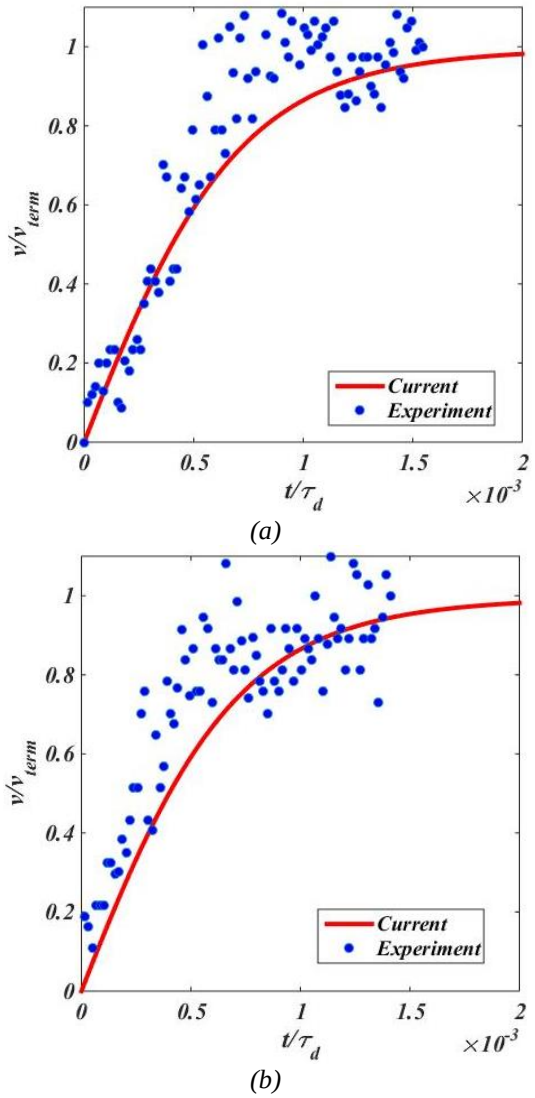

Fig. 13: Transient behavior to steady-state ($Re_{p,term}$ ~11590, S~2.2) for (a) Run#9a (b) Run#9b

Generally speaking, the results are in good agreement with the code predictions. The presentation of the results on a dimensional scale will reveal the actual differences in the transient behavior which are mostly because of the presence of the nearby wall. At a lower frame rate less scatter in the data is observed possibly because of the higher resolution obtained by the camera at a lower frame rate. An even higher frame rate (~1000 fps) sacrifices the image resolution and makes it difficult for the software to perform the tracking process. Moreover, using the wider cylinder compromises the transparency of the fluid and thus makes it more challenging to identify the borders of the moving sphere. This is the reason for having more scatter in the wide cylinder as compared to the narrow one. In addition to that, the transparent glass sphere is harder to track compared to steel spheres (Runs 4, 8, and 9). Although the scatter of the values of velocities may make it challenging to judge the agreement in some cases reasonable agreement can be seen in the results in non-dimensional scales.

4.2 Influence of the wall

Many researchers suggested different correlations for the correction factor of the drag coefficient of a single sphere falling in a cylindrical container [12, 13]. The correction factor considered in this work takes the form

$$F(r) = CD_w/CD \quad (6)$$

In Eq. (6), CD_w is the drag coefficient of a single sphere falling in a cylinder of finite diameter. $F(r)$ is the correction factor and takes values of ≥1 and r is the diameter ratio (d/D). Below are two selected correlations for a comparison purpose. These are Landenburg's formula and Haberman & Sayre's formula's respectively:

$$F(r) = 1 + 2.4r \quad (6a)$$

$$F(r) = \frac{1 - 0.75857r^5}{1 - 2.105r + 2.0865r^3 - 1.7068r^5 + 0.72603r^6} \quad (6b)$$

The selected correlations almost bracket or are about the same as other correlations and thus can indicate the dispersion in the correlations themselves. It should be noted that Landenburg's formula has an applicability limit or r ≤ 0.1 whearas Haberman & Sayre's formula has an applicability limit of r ≤ 0.5

Four experiments are selected to investigate the effect of the wall; Run #1 and 5 which both utilize the same ball at different cylinder diameters. Figure 14 presents a side-by-side comparison of the two cases along with the transient solution when the wall correction factor (selected formulas) is included. As can be seen that the predicted wall correction effect of Run#1 seem to be over-predicted even for Landenburg formula which is less strict than Haberman & Sayre. When the diameter ratio goes less than 10 % (Run#5), both selected wall correction formulas tend to give similar predictions (such as shown in Figure 14b). However, the experiment is in agreement with the code predictions without the influence of the wall as presented by the red solid line.

Figure 15 *a* and *b* shows a comparison of the transient behavior for the narrow graduated cylinder at two different terminal Reynolds numbers. Both experiments have almost the same sphere/cylinder ratio. The terminal Reynolds number of Run 2a is ~ 44 and is ~13 for Run#4. Both results agree with Landenburg correction factor with Run#2a seemingly slightly over-predicted as compared to Landenberg formula. The reduction of the wall effect with the increase of Reynolds number is suggested by the graphical method of Fidler & Whitmore [14].

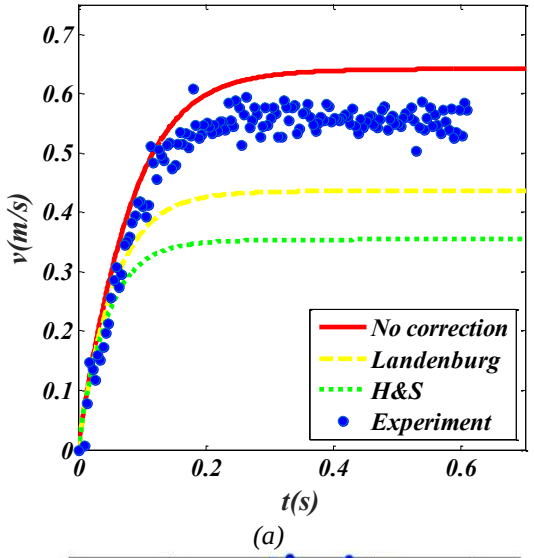

(a)

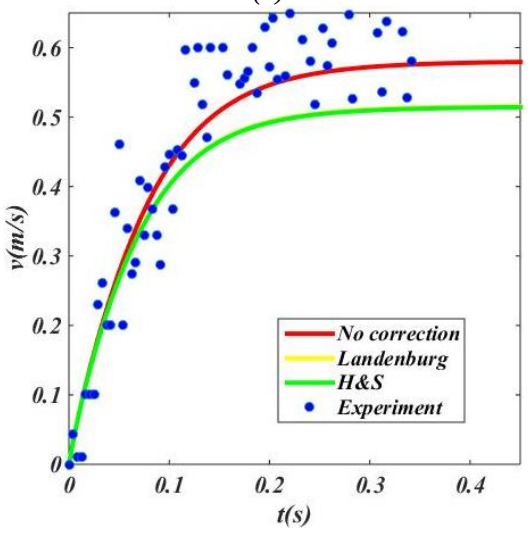

(b)

Fig. 14: Comparison of the transient behavior for narrow and wide cylinders of (a) Run#1 (b) Run#5

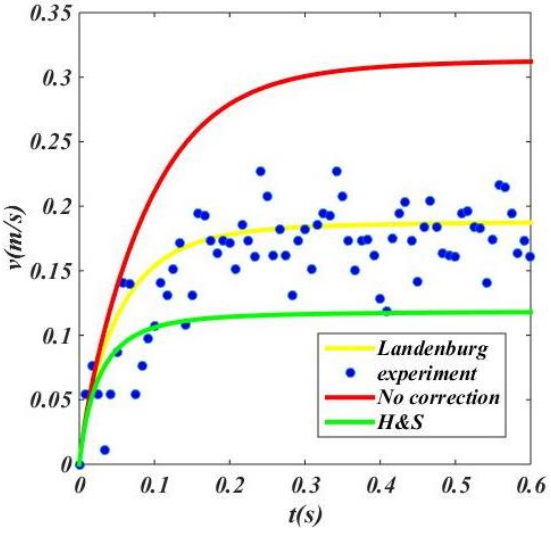

(a)

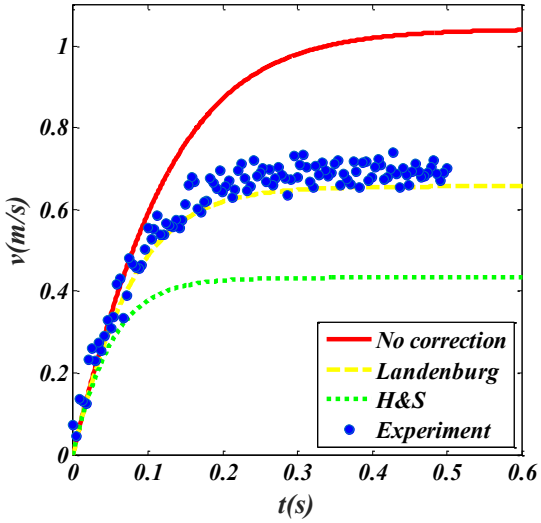

(b)

Fig. 15: Comparison of the transient behavior of settling spheres at narrow cylinders at different terminal Reynolds numbers with and without wall effect correction *a)* Run#4 *b)* Run#2a

4.3 Uncertainty in the experimental results

Other than the wall effect, uncertainty may come from the estimation of the fluid properties (viscosity and density) or even the sphere diameter. Another factor that should be considered is the determination of the onset of release. In fact, uncertainties cause deviations between the experiment and theory and the total deviation is an artifact of the accumulation of all of these uncertainties.

In the current work, we measured the diameter of the spheres with a micrometer with an accuracy of 0.1 mm. The diameters reported by the manufacturer of the falling ball viscometer (Table 2) were in very good agreement with our own measurements. Similarly, the mass of the spheres was measured with an accuracy of ±0.001 *g* and was in good agreement with the values provided in the ball kit (differences are less than 0.2%). The maximum deviations observed were in the fluid kinematic viscosity which in one case was up to about 8% as reported by the manufacturer. The former difference with the typical data is not of real concern since the reported specification can be affected by allowable production tolerance. Such difference in viscosity is found to be insignificant when the terminal velocity is of interest. We also admit that the release mechanism may make the initial velocity to be slightly different than zero. It should be mentioned that deviations between the experiment and predicted values can also be due to uncertainties in force models (e.g., drag and history force models).

To investigate the influence of uncertainty in the transient behavior of a settling sphere we selected Run#1 and assumed uncertainty in the kinematic viscosity of ±10%,

uncertainty in sphere density of ±10%, and sphere diameter of 0.1 mm. The combined effect of all these uncertainties is shown in Figure 16 where the upper and lower uncertainty limits are obtained by including the maximum uncertainty of all the parameters that result in the same effect. It is noteworthy that in spite of the exaggerated uncertainty induced, the terminal velocity predicted by the simulation seems to be slightly affected. Marginal variation between the uncertainty limits can be noted in the transient behavior. The scatter of the data is an artifact of the image processing stage.

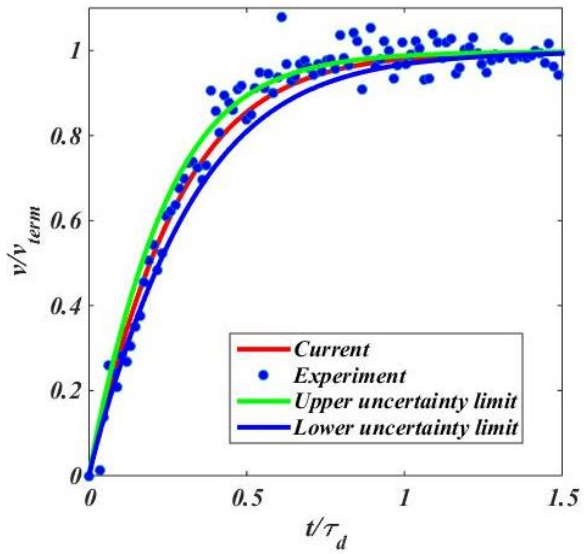

Fig. 16: Transient fall of the sphere (Run#1) with uncertainty limits of used parameters

5. Conclusions and Recommendations for Further Work

The equation that governs the motion of a spherical particle was solved numerically. The developed code showed good agreement when validated with published data at a wide range of Reynolds numbers and density ratios. Tracking the falling sphere is possible using a frame rate of 60fps is possible for Reynolds numbers of ~40 or less provided that the fluid transparency is adequate. For the used oil, the former condition was possible when the narrow cylinder is used, however, a water-glycerin mixture might be superior for this regard. At frame rates of 240 fps, the detection algorithm would have some noise which might be because of the insufficient resolution which makes it harder to identify the exact location of the sphere. In such cases, sub-pixel displacement becomes harder to identify and noise is added to the experimental data. The noise in the experimental data is higher for the wide cylinder and at a higher Reynold's number, and when glass spheres are used.

Although Tracker was easy to use and led to reasonably good agreement between the experiment and result it is recommended that an alternative image processing software/program be tested. The development of an in-house post-processing program or modification of the MATLAB® image processing toolbox is suggested. MATLAB® has an image processing toolbox that can detect objects but lacks the implementation of position calibration and post-processing. This may help increase the accuracy of location detection.

The use of a proper release mechanism of the ball rather than the manual release of the sphere. The release mechanism should be capable of reducing the error/uncertainty of the initial velocity (which should be zero). And if a –laser- beam/light can be in the video scene which turns off at the release instant this may help in the identification of the release moment. Since the rotation of the sphere affects the wall correction factor [12] the experimental part would benefit from adding a method of identification of the rotation of the spheres (e.g. by marking or colorizing their view).

The deviations of the current experiments with the code predictions are mostly because of the wall correction. The correction factor of Landenburg resulted in better agreement with the current experiments at a sphere to cylinder ratio (d/D) of ~ 30-40%. Nevertheless, it was found to over-predict the results in some cases especially with the d/D ratio decreasing to less than 10%. Although Reynolds number is not included in most of the wall correction factor formulas, the authors suggest that the correction factor should be a function of Reynolds numbers along with the diameter ratio. The former conclusion was also suggested by [14], however, the suggested graphical method to estimate the correction factor made it less attractive to be used.

Using CFD (resolved surface approach) to validate the results, especially in cases with wall effect. This can help in identifying which wall-correction factor correlation is recommended in use and possibly lead to the development of a new correlation. This part may be performed using existing software/programs.

Acknowledgement

The authors would like to acknowledge the co-operation of Eng. Ramadan Alwerfalli co-coordinator of the Mechanical Engineering department laboratories for his co-operation in providing measurement facilities to be used by the current work.

References

[1] Moorman, R.W., Motion of a spherical particle in the accelerated portion of free fall. The University of Iowa.1955

[2] Mordant, N. and J.-F. Pinton, Velocity measurement of a settling sphere. The European Physical Journal B-Condensed

Matter and Complex Systems, 18(2): p. 343-352, 2000.
[3] Ten Cate, A., C. Nieuwstad, J. Derksen, and H. Van den Akker, Particle imaging velocimetry experiments and lattice-Boltzmann simulations on a single sphere settling under gravity. Physics of Fluids, 14(11): p. 4012-4025, 2002.
[4] Rostami, M., A. ARDESHIR, G. Ahmadi, and P.J. Thomas, Can the history force be neglected for the motion of particles at high subcritical Reynolds number range? 2006.
[5] Hedayati Nasab, S., Free Falling of Spheres in a Quiescent Fluid, Concordia University, 2017.
[6] Akhlis, I., M. Syaifurrozaq, P. Marwoto, and R. Iswari. The determination of fluid viscosity using tracker-assisted falling ball viscosimeter. in Journal of Physics: Conference Series, IOP Publishing, 2010.
[7] Loth, E. and A.J. Dorgan, An equation of motion for particles of finite Reynolds number and size. Environmental fluid mechanics, 9(2): p. 187-206, 2009.
[8] Clift, R., J.R. Grace, and M.E. Weber, Bubbles, drops, and particles, 2005.
[9] Mei, R. and R.J. Adrian, Flow past a sphere with an oscillation in the free-stream velocity and unsteady drag at finite Reynolds number. Journal of Fluid Mechanics, 237: p. 323-341, 1992.
[10] Loth, E., Particles, drops and bubbles: Fluid dynamics and numerical methods. Particles, Drops and Bubbles: Fluid Dynamics and Numerical Methods, 2010.
[11] Tracker. Tracker: Video Analysis and Modeling Tool. [cited 2019 9/15/2019]; Tracker: Video Analysis and Modeling Tool]. Available from: http://www.cabrillo.edu/~dbrown/tracker/.
[12] Haberman, W. and R. Sayre, David Taylor Model Basin Report No. 1143, Washington, D. C, US Navy Dept, 1958.
[13] Li, M., G. Zhang, J. Xue, Y. Li, and S. Tang, Prediction of the wall factor of arbitrary particle settling through various fluid media in a cylindrical tube using artificial intelligence. The Scientific World Journal, 2014.
[14] Fidleris, V. and R. Whitmore, Experimental determination of the wall effect for spheres falling axially in cylindrical vessels. British journal of applied physics, 12(9): p. 490, 1961.